EUROPEAN ORGANIZATION FOR NUCLEAR RESEARCH

CERN EP/79-15
27 February 1979

INELASTIC HADRON-NUCLEUS INTERACTIONS AT 20 AND 37 GeV/c

M.A. Faessler, U. Lynen, J. Niewisch*),
B. Pietrzyk, B. Povh and H. Schröder**)

Max-Planck-Institut für Kernphysik,
Physikalisches Institut der Universität Heidelberg, Heidelberg, Germany

CERN, Geneva, Switzerland

P. Gugelot

Department of Physics, University of Virginia
Charlottesville, VA, USA

T. Siemiarczuk and I.P. Zielinski

Institute of Nuclear Research, Warsaw University, Warsaw, Poland

(Submitted to Nuclear Physics B)

*) Present address: Siemens AG, Erlangen, Germany.

**) Present address: DESY, Hamburg, Germany.

ABSTRACT

The experiment studied charged particle production for π^-, K^-, and $\bar{p}$ interactions on nuclei at 20 and 37 GeV/c at the CERN SPS. A non-magnetic detector, consisting of CsI(Tl) scintillation and lucite Čerenkov counters, distinguishes between fast particles, mainly pions, and slow particles, mainly nucleons, with a cut at velocity $\beta \approx 0.7$. Angular distributions, multiplicity distributions of slow and fast particles were analysed. It is shown that the measurement of the correlations can provide a critical test for different theoretical models of the hadron-nucleus interaction. At the energies studied so far a systematic deviation from KNO scaling is observed. This gives further support to the "standard picture" of the hadron-nucleus interaction and it contrasts with predictions of the coherent tube model. The regularity observed for the angular distribution of fast secondaries as a function of the number of slow particles can only be explained by combining features predicted by different models.

1. INTRODUCTION

It has been realized for a long time that the study of inelastic hadron-nucleus interactions at high energies can serve as a test of models for the hadron-nucleon interaction and might provide additional information on the strong interaction of hadrons which cannot be obtained by studying hadron-nucleon interactions alone. Characteristic times of strong interactions are of the order of 1 fm/c. This is the minimum time it takes a pion to be emitted in its rest frame; for a fast moving pion this time is Lorentz-dilated. The propagation time of relativistic hadrons through nuclei, however, amounts to a few fm/c, depending on the thickness of the nucleus. Thus, if one pictures the interaction of a hadron with a nucleus as a sequence of several collisions with nucleons, the time between the collisions is comparable to or smaller than the Lorentz-dilated characteristic time. Therefore an excited hadron *in statu nascendi*, rather than the final particles emerging from an interaction, collides with subsequent nucleons. It is about this early state of excited hadronic matter than one hopes to learn by examining inelastic hadron-nucleus interactions at high energies.

Historically, high-energy interactions have first been observed on nuclei. Before accelerators became available, the easiest way to study them was to expose emulsions to cosmic rays. It was hoped that the hadron-nucleus interaction does not differ much from the hadron-nucleon interaction. In fact, there is very little difference for the majority of events. At the presently operating accelerators most experiments have been carried out with a proton target, since highest priority was given to understanding the simplest system accessible -- the hadron-proton system.

Thus many, in fact, most experimental data on inelastic hadron-nucleus interactions were provided by measurements in emulsions. The disadvantage of having a mixture of target nuclei in the emulsion is partly compensated by the manifestation of the nuclear response in the tracks of nuclear fragments, the "black" tracks (kinetic energies $E_{kin} < 30$ MeV) and the "grey" tracks ($30 < E_{kin} < 500$ MeV). At high energies above 20 GeV a linear relation between the mean number $\langle N_s \rangle$ of fast particles and the number of heavy tracks N_h (the sum of grey and black tracks) was

found, and it was believed that N_h represents some measure of the number ν of collisions within the nucleus [1].

Having a measure of the number of collisions within the nucleus on an event-to-event basis is, of course, better than just knowing the target mass. In the latter case one can calculate the mean number of collisions, but one would obtain an average over all kinds of collisions, from peripheral to central ones.

The experiment described here attempts to combine the advantages of an electronic detector, which can collect large data samples on a target with well-defined mass number, with the advantage of the emulsion experiment, which can measure the nuclear response by detecting black or grey tracks. It was conjectured that the correlation with the number of collisions in the nucleus would be stronger for grey tracks than for black ones, because the recoil nucleons are expected to appear as grey tracks, while the black tracks are evaporation products and therefore less directly related to the primary collisions. More importance was thus attributed to the detection of grey tracks.

To this end a non-magnetic detector was built that covers 50% of the total solid angle, sufficiently subdivided in angle to measure multiplicities of charged particles and with the ability to discriminate between fast and slow particles. The separation point between fast and slow is a velocity somewhat above $\beta = 0.7$, which corresponds to the separation between fast (= shower) particles and heavy tracks of emulsion experiments. The lower cut-off in the energy of slow particles is determined by absorbing material in front of the counters and by absorption in the target.

Another aim of the experiment was to study the energy and projectile dependence of particle production off nuclei in the energy range between 20 and 100 GeV. In this range less data exist than for incoming energies above 100 GeV and below 20 GeV. The data imply that $R = \langle N_s \rangle_{em} / \langle N_{ch} \rangle_{pp}$, the number of fast particles $\langle N_s \rangle$ produced on emulsion nuclei normalized to the charged particle multiplicity $\langle N_{ch} \rangle$ of pp interactions at the same energy, first rises between 20 GeV and 100 GeV incoming energy and then seems to remain constant, at the remarkably low value around

1.8 up to the highest measured energy [1]. The above-mentioned dependence of $\langle N_s \rangle$ on N_h changes from no correlation at 10 GeV/c incoming momentum to a linear dependence

$$\langle N_s \rangle = \alpha N_h + \beta \ , \tag{1}$$

with increasing slope ($\alpha \approx 1$ at 60 GeV/c). These two results indicate that the energy region between 20 and 100 GeV is a region of transition. The slow rise or constancy of R above 100 GeV/c is widely believed to be due to the fact that the Lorentz-dilated evolution time of the produced hadronic system is much larger than the propagation time through the nucleus. On the other hand, at low energies, the produced hadrons could reach their final state already within the nucleus and a multiplication of secondaries, an intranuclear cascade, could occur. This effect, if it exists, will certainly be obscured by the constraint that at low energies the secondaries do not have sufficient energies to multiply. At high energies the experimental number of produced secondaries is generally much smaller than energetically possible, so there is no such constraint.

Therefore a closer examination of the energy dependence in this region, and of the projectile dependence for similar reasons, seems worthwhile.

We will refer in the text several times to the "standard picture" of the hadron nucleus interaction. This is simply a common feature of most models. Assume that the nucleus is at rest in the laboratory system. According to the "standard picture" the secondaries can be divided into two components. The first component is the secondaries at low energies. Their number increases linearly with the number of target nucleons hit by the projectile; each collision contributes a statistically independent amount to the sum of low-energy secondaries. The second component, consisting of high-energy secondaries, is essentially independent of the number of collisions. The "critical" energy E_c which separates the two components, depends either on the maximum energy, i.e. the incoming energy, or on the size of the nucleus.

2. THE DETECTOR

The slow and fast particles are separated by means of a combined counter consisting of a CsI(Tl) crystal, 3 mm thick with a diameter of 50 mm, which is glued to a lucite light-guide. The CsI crystal scintillates proportionally to the energy loss of the particles in the crystal, and if the velocity is bigger than $\beta = 1/n \approx 0.7$, n being the refraction index of lucite, the lucite light-guide acts as a Čerenkov radiator. The anode signal evoked by the Čerenkov radiator is a short pulse, around 500 mV high for a typical amplification of the phototube, whereas the CsI produces a long signal, 50 mV high for minimum ionizing particles, with a decay time of 1 μsec. The rise-times of the CsI and Čerenkov pulses are different; the latter is determined by the intrinsic resolving time of the tube and signal cable, while the CsI crystal has a rise-time of typically 30 nsec. This difference is utilized for separating fast and slow particles in the off-line analysis. The anode signal is split between a discriminator and an analogue-to-digital converter (ADC). The outputs of the discriminator are led to a time-to-digital converter (TDC) and a pattern. TDC and ADC (energy loss) of each counter are recorded on tape together with the pattern information.

Seventy-three of these combined counters cover 52% of the total solid angle and form seven rings of roughly equal size in pseudorapidity $\eta = -\ln \operatorname{tg} \theta/2$, θ being the polar angle with respect to the beam axis (Fig. 1). There are no counters between $\theta = 180°$ and $\theta = 165°$. The forward direction ($\theta < 13°$) is covered by four rings of a lucite counter hodoscope, and one lucite counter is situated at $\theta = 0°$. Since the forward cone represents only 1% of the total solid angle and recoil nucleons moving forward are expected to be mostly fast in any case, the discrimination between fast and slow particles is considered to be irrelevant.

The unseparated S1 beam at the CERN SPS was used [2]. Two gas Čerenkov counters $\check{C}_1$ and $\check{C}_2$ served to distinguish between π, K, and p; one was 5 m long and filled with N_2 at 37 GeV/c and with freon at 20 GeV/c, and the other was 8 m long, filled with a He-Ne mixture at 37 GeV/c and with N_2 at 20 GeV/c. In the former K and π were detected above threshold and in the latter only π. Protons are marked by the absence of a signal in both counters. The pion signal contains

an unknown fraction of electrons, extrapolated to be smaller than 13% (4%) for 20 GeV/c (37 GeV/c) from measurements at the same beam [3]. Electrons will interact electromagnetically with high probability, especially in the heavy targets; but they lead to low multiplicity events and are unlikely to be accepted by our trigger. Since we did not aim at absolute cross-section measurements, they were considered as harmless.

The beam was defined by counter B (5×10 cm^2) in front of $\check{C}_1$, counter S (5×10 cm^2) between $\check{C}_1$ and $\check{C}_2$, and counter D (1×1 cm^2, 1 mm thick) (Fig. 1). The final definition of the beam spot was accomplished by a veto counter A_H with a $\phi = 8$ mm hole to minimize unrecognized interactions upstream of the target, in the gas of the Čerenkov counters, the vacuum windows, and the beam defining counters. Two large veto counters A_L and A_R covered the active area of the detector to reject halo particles arriving simultaneously with a beam particle. A counter A_B was installed 40 m downstream of the target behind several quadrupoles and a bending magnet serving as additional beam-veto counter.

3. RUNNING CONDITIONS

The trigger was "Beam" × "Or", where "Beam" is defined as $B \cdot S \cdot D \cdot \bar{A}_H \cdot f(\check{C}_1,\check{C}_2)$, $f(\check{C}_1,\check{C}_2)$ being a combination of the gas Čerenkov counters to select the desired beam particles. This trigger was vetoed by A_B -- at the CAMAC level, because the A_B signal arrived late. To obtain roughly the same statistics for π, K, or p, one third of the data was accumulated without any Čerenkov counters in the trigger (π, K, p runs) and two thirds with $f(\check{C}_1,\check{C}_2) = \bar{\check{C}}_1$ (K, p runs). See Table 1 for the relative intensity of beam particles at the different energies.

In most runs "Or" required any two of the vertex counters, except the counter at 0° which was not included in the trigger. Requiring only one counter alone would have given too high a background due to accidental coincidences.

Following a trigger signal the patterns were read first and only then were the TDCs and ADCs, of the vertex counters that had fired, written on tape. This was done to reduce the amount of written data.

The beam intensity was chosen to yield as high a number of triggers per burst as could be accepted by the computer. Typical rates are listed in Table 2. The main data were taken at two energies, 20 and 37.5 GeV/c, with negative polarity. The targets examined were ^{12}C (4 mm), ^{27}Al (4 mm), ^{64}Cu (2 mm), ^{108}Ag (2 mm), and ^{207}Pb (2 mm). (The target thickness is given in brackets.) The diameters were between 10 and 15 mm. In addition, measurements with a Pb target 5 mm thick and with an empty target position were taken for each energy.

The choice of target thickness was somewhat difficult. A thick target is desirable to improve the signal-to-background ratio, the background originating from interactions in the air and from accidental coincidences; and a thin target is needed to keep secondary interactions in the target low. An additional requirement for the target was to absorb the low-energy fragments from nuclear evaporation. Targets with a thickness of 1% absorption length seemed to be a good compromise.

4. ANALYSIS

The first step in the analysis consists of determining the precise timing of prompt particles of all 136 counters involved (including the beam counters) using the TDC spectra. For the combined counters the TDC spectra display two peaks, one due to the Čerenkov signal produced by the prompt, fast pions, and a second one due to the CsI signal produced by slow particles which do not give Čerenkov light. Both peak positions are marked. After the time constants have been determined, the time gate, which is 50 nsec long in the hardware trigger, can be reduced to 6 nsec. The fast and slow particles are separated by cutting in the TDC along the valley between the pion peak and the peak of slow particles, taking into account the time slew at low pulse heights known from the two-dimensional TDC versus ADC spectra.

A cut in pulse height was applied below the peak of minimum ionizing particles, because the combined counters could fire for other reasons than a charged particle originating from the target, e.g. a photon interacting in the lucite cone or particles entering through the side of the counters without hitting the CsI

crystal; electronic cross talk was another reason. A cut about two standard deviations below and above the peak of single particles had to be applied for the $\check{C}$ hodoscope counters to suppress the background induced by photon conversions, electronic cross talk, and δ rays.

We will use the term "observed number" of fast or slow particles for the rates found after these initial cuts. We then corrected all rates for acceptance in solid angle and obtained pseudorapidity distributions of fast particles and angular distributions of slow particles as functions of target, projectile, projectile energy, observed number of fast and slow particles.

The TDC and ADC information of the beam counters was used to clean the "Beam" trigger further and to identify projectile particles. Any event having a signal in one of the large veto counters A_L or A_R was rejected.

Owing to the rejection of accidental counts, some of the events surviving the previous cuts were again of low multiplicity $N_s + N_g < 2$. Those events were rejected, since they were not accepted by the hardware trigger. No corrections were applied for the missing events with multiplicity < 2 when we calculated the mean values.

Since the resolution of the counters was not sufficient to identify double hits by the measured pulse height, the multiplicity was corrected for double and multiple hits in one counter. It was assumed that multiple hits occurred only on a statistical basis. The corrections amount to less than +10% for the highest observed fast multiplicities ($\sim$ 13) and to less than +4% for average multiplicities ($\sim$ 7).

The finite target thickness was taken into account. Finite target thickness has two effects: firstly, the frequency of events with high multiplicity is increased by secondary interactions in the target; and secondly, slow particles are absorbed in the target. The main contribution to secondary interactions in heavy targets is due to conversions of γ's from π^0 decay. It was assumed that the $\pi^0/(\pi^+ + \pi^-)$ production ratio is constant and equal to 0.5 and the γ angular distribution is the same as that of charged $\pi^{\pm}$; this last assumption is certainly

bad for large laboratory angles and consequently the background subtraction will somewhat distort the pseudorapidity distribution around $\eta = 0$. This correction thus depends on the observed number of fast particles emitted into a given angle and on the target geometry in units of radiation lengths. The secondary interactions of charged pions were assumed to be only rate-dependent: if d is the target thickness in units of absorption lengths and E the incoming energy, the correction applied was

$$\Delta\langle N_s\rangle_d = -\frac{d}{2}\langle N_s(E)\rangle\{\langle N_s(E/N_s)\rangle - 1\} . \qquad (2)$$

The magnitude of the target-thickness correction could be compared with measurements from the Pb target, where two thicknesses, 2 mm and 5 mm, have been used; and it agreed well.

The empty-target measurement revealed two kinds of background: a contribution from accidental coincidences at low multiplicities and a contribution from interactions, including δ-ray production, in the air in front of and behind the target position. The former depends, of course, on beam intensity and duty cycle; the latter occurs at a 25% level of the interactions in the target contributing mainly at low multiplicities and small angles, because behind the target a longer path through air has to be traversed by the beam within the detector than in front of the target. The empty-target events have been subtracted, properly normalized, from all data; but the accidental background could not be dealt with satisfactorily, since beam intensity and duty cycle of the machine varied considerably, especially in the runs during the early days of the SPS. This causes a considerable uncertainty in cross-section for events without slow particles and with less than four fast particles, as we can see by comparing different runs. Consequently, those mean values which are mainly based on the above events contain large systematic errors. If possible, we selected samples with a small estimated error of this nature.

Finally, a slight (< 10%) mismatch was found in the particle rates in the $\check{C}$ hodoscope and the combined counters. This was corrected for by assuming that the pseudorapidity distribution of fast particles, for events with no slow particle

and with 5-8 fast particles, is symmetric around 90° in the c.m. system of the projectile-nucleon system. The correction factors obtained in this way were applied to all rates in the forward hodoscope. One has to keep in mind that the whole pseudorapidity distribution, even for a pp collision, should be slightly asymmetric owing to several effects. At low laboratory rapidities pions are lost, being identified as slow particles; and at high rapidities a forward target nucleon with sufficient recoil momentum will add to the fast particles. Moreover, the pseudorapidity distribution is distorted, again in such a way that high rapidities are favoured, since the laboratory angle corresponding to 90° in the c.m. depends on p_T, according to the following formula:

$$\text{tg } \theta \text{ (90° c.m.)} = \frac{\sqrt{1 - \beta_{cm}^2}}{\beta_{cm}} \frac{p_T}{m_T} . \qquad (3)$$

4. RESULTS

4.1 Characteristics of slow particles

We first want to demonstrate that the slow particles are essentially the same as the "grey" particles of emulsions with some admixture of "black" tracks.

In emulsions, grey tracks are mostly defined to have velocities between 0.3 and 0.7. Our upper cut in velocity, somewhat above $0.7 = 1/n_{lucite}$, is thus almost identical with the one in emulsion. In this experiment the lower cut-off is given by the target thickness and the material in front of the CsI crystal (10 to 30 cm air plus 2 mm lucite) which stops most of the very slow particles, the black tracks. By means of their measured energy-loss distribution in the CsI crystal (and knowing dE/dx), we have some crude information on the energy distribution of the slow particles. An ambiguity is caused by particles that stop in the CsI crystal. To determine the fraction of black tracks we also placed additional absorbers in front of the counters (8.5 mm of lucite corresponding to the range of 32 MeV protons) for a few runs. The over-all mean of slow particles is then shifted by 13%. In Fig. 2 the angular distribution $dNg/d\Omega$ as a function of the energy loss is shown for the lead target (2 mm thick). The dip at 90° is due to

absorption in the target. With increasing energy loss, i.e. decreasing energy, the forward/backward ratio decreases. This behaviour, together with the energy-loss distribution and the change with additional absorbers, is quite consistent with the assumption that the majority of slow particles are grey tracks, i.e. protons.

We now come to those properties of the slow particles that are relevant for their interpretation as a measure of the number of collisions in the nucleus. Figure 3a shows the frequency of events $f(N_g,A)$ versus the number of observed slow particles for different targets at 37 GeV/c. While π^- and K^- have equal distributions, $\bar{p}$ shows a slower fall-off with N_g. The distributions are substantially broadening with increasing target mass and they are energy independent between 20 and 37 GeV/c to a remarkably high degree, as can be seen in Fig. 4a where the ratio

$$R(N_g,\ A,\ 37.5/20) = f(N_g,\ A,\ E = 37.5\ \text{GeV})/f(N_g,\ A,\ E = 20\ \text{GeV}) \qquad (4)$$

is plotted. This latter property has been known from emulsions [4] to apply to a much wider energy range, and it was one of the reasons to assume that N_g could serve as a measure for the number of collisions in nuclei. It is interesting to note that the low-energy part of the fast particles (small $\eta = -\ln \text{tg}\ \theta/2$) is energy independent as well (see next section and Fig. 6b). Hence there is a smooth transition of the energy dependence going from slow to fast particles. No significantly different target mass dependence was found for the mean values of slow and fast particles, as can be seen in Fig. 5, where the mean values are plotted versus the mean number $\bar{\nu}$ of collisions in the nucleus calculated as

$$\bar{\nu} = A\sigma_{\pi N}/\sigma_{\pi A}\ , \qquad (5)$$

with $\sigma_{\pi N}$ and $\sigma_{\pi A}$ being the inelastic cross-sections of pions on a nucleon and a nuclear target with mass A, respectively.

4.2 Characteristics of fast particles

The energy-loss distribution of fast particles is quite different from that of slow particles. It is consistent with a Landau distribution of minimum ionizing particles and independent of angle, incoming energy, target mass, and projectile.

In the following we will discuss the properties of the fast particles as if we had measured only them. Apart from the slightly different trigger bias and the different incoming energies, the data in this form can be compared with experiments which do not measure the nuclear response. Thus we have the possibility of checking part of our data with existing data.

The distribution of events $f(N_s, A)$ versus the observed number of fast particles is shown in Fig. 3b for different targets and for 37.5 GeV/c. Contrary to slow particles, the distributions are not only target- but also energy-dependent. The energy dependence can be seen by plotting the ratio

$$R(N_s, A, 37.5/20) = f(N_s, A, E = 37.5 \text{ GeV})/f(N_s, A, E = 20 \text{ GeV}) \ . \qquad (6)$$

As one would expect, the number of events with high multiplicity increases faster -- with increasing energy -- the higher the multiplicity (Fig. 4b).

The pseudorapidity (η) distribution $[\eta = -\ln \text{tg}(\theta_{lab}/2)]$ shows the familiar increase with increasing target mass at lower values of η (Fig. 6a). That of carbon, the lightest target used, is expected to resemble very much the hadron-nucleon distribution. Comparing these η distributions with other experiments carried out at the same energy [5-7] or at an adjacent energy (50 GeV), good agreement is found between our measurement with the Ag-target and the η distribution for Ag and Br nuclei from emulsion experiments [5], whereas large discrepancies exist between our measurement for the Pb-target and other experiments [6,7], especially at low η. There are even stronger discrepancies if one compares the two other experiments with each other.

The target dependence of the rapidity distributions is displayed somewhat differently in Fig. 7, where the variation of $dN_s/d\eta$ versus $\bar{\nu}$ is plotted separately for all η bins. From this figure we can extract the normalized slope $S(\eta)$ (Fig. 8),

$$S(\eta) = \frac{d^2\langle N_s \rangle}{d\eta d\bar{\nu}} \Big/ \frac{d\langle N_s \rangle_{\nu=1}}{d\eta} \ , \qquad (7)$$

which is of special interest, since most theoretical models of particle production by nuclei predict only the relative increase of secondaries compared to the η-distribution for pp collisions ($\nu = 1$).

$S(\eta)$ being equal to one would signify that in the following collisions the same numbers of secondaries per collision as in the first collision are emitted into the angle η. According to the "standard picture" $S(\eta)$ is equal to one for η smaller than a certain critical value η_c and equal to zero for η bigger than η_c. Thus the "standard picture" has to be somewhat revised by the fact that $S(\eta)$ is bigger than one for small η, which could indicate intranuclear cascading of the low-energy secondaries and $S(\eta)$ being smaller than zero for high η, which corresponds to depletion of the fast forward particles and will be discussed in more detail below. The slope of the highest and lowest measured η bin could not be determined well for the large systematic error associated with these points. For the lowest η bin this is due to the $\pi^0 \to \gamma$ background subtraction and for the highest bin it is due to the uncertainty of the empty target background subtraction. Since low-multiplicity events contribute most to the highest η, it would require very careful cross-section normalization, which we have not done, or equal running conditions for different targets, which we have not had either, to make a safe statement about the quantitative behaviour at the highest η. We will show below that there is a depletion at high η with increasing number of slow particles, which in a way is equivalent to increasing the target mass.

The energy dependence as a function of η at fixed target mass is shown in Fig. 6b. Here the ratio

$$R(dN_s/d\eta,\ A,\ 37.5/20) = \frac{d\langle N_s\rangle_{37.5\ GeV}}{d\eta} \Big/ \frac{d\langle N_s\rangle_{20\ GeV}}{d\eta} \qquad (8)$$

is plotted. Below $\eta = 1$, R is equal to 1, thus indicating energy independence. We mentioned already that this seems to be a universal property of the target fragmentation region, applying also to the slow particles. The two highest η points and the lowest one deviate from the general trend, which again reflects the large experimental uncertainty associated with these points. The ratio R at low η deviates for the silver target from 1.0 by 20%, but we attribute this to a systematic error in the cross-section normalization.

4.3 Correlations between fast and slow particles

In this section we will deal with the principal results of the present experiment, the correlations between fast and slow particles.

Let us consider the frequency distribution $f(N_s,N_g)$ of events, where N_s and N_g are the observed multiplicities of fast and slow particles (Fig. 9). The remarkable feature of these curves is that the ratio

$$Z = \sqrt{\langle N_s^2\rangle - \langle N_s\rangle^2}/\langle N_s\rangle = \langle D(N_s)\rangle/\langle N_s\rangle. \qquad (9)$$

(with the denominator $\langle D(N_s)\rangle$ being the mean dispersion) decreases with an increasing number of slow particles (Fig. 10b). This is a behaviour quite different from that observed for the dispersion as a function of target mass and energy when averaged over N_g. In the latter case the value of Z is consistent with constancy. It varies between 0.52 and 0.58 randomly; most likely the variations are due to the above-mentioned uncertainty for the cross-section of low multiplicity events. But when the number of fast particles is increased as a function of N_g, Z decreases systematically. This is shown in Fig. 10a, where the ratio is plotted versus the corrected mean value $\langle N_s\rangle$ for different energies and different targets averaged over N_g (crosses between 0.52 and 0.58; also shown is the region where points from the experiment at FNAL [6] are located), and for $\langle N_s\rangle$ increasing as a function of N_g (the latter points are connected by lines. The mean values $\langle N_s\rangle$ used here are the ones corrected for solid angle, etc., and the dependence of $\langle N_s\rangle$ on N_g will be shown below in Fig. 11.). For events with very high multiplicity of both fast and slow particles the total number of tracks represents already a considerable fraction of the counters in the detector; thus the ratio Z will be decreased owing to multiple hits in one counter, but this effect is estimated to be small. It can be seen from a comparison of the 20 and 37.5 GeV data for Pb, which have significantly different average multiplicities (Fig. 10a), that the absolute multiplicity in first approximation does not affect the systematic decrease of Z with N_g (Fig. 10b). For pp interactions the energy independence of Z over an energy range as wide as 9 to 10^4 GeV/c was observed by

Malhotra a long time ago [8]. Gurtu et al. [1] and Babecki et al [9] found a significant decrease of the ratio Z in emulsion experiments, i.e. for hadron-nucleus interactions, with increasing N_h, an effect which could only partly be explained by the composite nature of the emulsion.

Qualitatively, the dispersion of the slow particles shows the same behaviour: $\langle D(N_g)\rangle/\langle N_g\rangle$ decreases as a function of N_s.

Figure 11 shows the corrected mean number of fast particles (we recall that this is the integral over a pseudorapidity distribution, corrected for acceptance, etc.) versus the observed number of slow particles for different targets and energies. Apparently, the mean values $\langle N_s\rangle$ increase with increasing N_g, and they reach a plateau at high N_g, at least for the higher target masses. There has been some indication of a plateau in earlier (emulsion) experiments [10]. Less direct experimental evidence exists for the target dependence of the correlation between fast and slow particles from emulsion experiments. This dependence, however, is expected, since the primary recoil nucleon, which has a high cross-section and is emitted normally at large angles, is likely to start a (slow!) intranuclear cascade [11]. From Fig. 11 and from the dependence $\langle N_g\rangle$ versus $\bar{\nu}$ (Fig. 5), which is compatible with a linear dependence, one can conclude that the A dependence of the correlation itself is only weak.

Finally, the change of pseudorapidity distributions with the observed number of slow particles is presented for the lead target and incoming momenta of 20 and 37.5 GeV (Fig. 12). An apparent structure of these dependences can be seen. At low rapidities, fast particles increase with increasing number of slow particles. In going to higher values of η, the curves reverse their slope at a certain number N_g, and the number of fast particles in the particular η bin starts to decrease with increasing N_g; the bigger η, the earlier the point of reversal. At lower incoming energy the depletion of fast particles extends further down in rapidity for fixed N_g or the point of reversal is reached after a smaller number of N_g, at a given η.

5. DISCUSSION

Our primary task will be to relate the number of slow particles N_g quantitatively to the number of collisions ν in the nucleus. As we have shown above, the definition of slow particles in this experiment is almost identical with that of grey tracks in emulsions.

Emulsion physicists have interpreted the grey tracks to be mainly protons (70-80%), with an admixture of slow pions (20%) and a small admixture of heavier evaporation products, and 20% are believed to be direct recoil protons [10]. If every slow particle were a charged recoil nucleon, one could immediately conclude that $\nu = \alpha \cdot N_g$ with $\alpha \gtrsim 2.0$, depending on the detection efficiency; but for the real mixture one has to allow a more complicated relation. Some attempts have already been made to find this relation for the grey tracks of emulsion [10,11]. It would exceed the framework of this paper to discuss these and to try to deduce the quantitative function $\bar{\nu}(N_g, A)$ for our case. Instead, for the following, only qualitative, discussion of our results it is sufficient to keep in mind that such a function exists and that $\bar{\nu}(N_g, A)$ is likely to be a monotonically rising function of N_g eventually saturating at high N_g.

In principle, one could bypass the problem of relating N_g to the number of collisions by interpreting N_g together with the number of pions at small η as a measure of violence of the target fragmentation in a more general sense. This interpretation is supported by the observation that the slow particles (N_g) and the fast particles at low pseudorapidity η behave very similarly with respect to target- and energy-dependence. If N_g was not too large it was found that $d\langle N_g\rangle/d\eta$ for small η rises linearly with N_g.

We can now proceed to discuss the behaviour of fast particles as a function of N_g, which is taken as a measure of the number of collisions or, more generally, as a measure of the violence of target fragmentation. Specifically we want to deal with two results, which, in our opinion, are a critical test for models of particle production on nuclei; one is the behaviour of the dispersion, and the other is the differential multiplicity $d\langle N_s\rangle/d\eta$ as a function of N_g and the incoming energy.

Several authors have noted [12-14] that the ratio $Z = \langle D(N_s)\rangle / \langle N_s \rangle$ should be a decreasing function of the number of collisions in the "standard picture" of the hadron-nucleus interaction. If, however, there is no difference between the collision of a hadron with a row or "tube" of ν nucleons at energy $\sqrt{s}$ and the collision of the hadron with a nucleon at a correspondingly higher energy $\sqrt{\nu s}$, as is claimed by the "collective tube" model [15], one would expect Z to be constant, since this is the case for the pp collisions independent of energy. Our observation of decreasing Z with increasing N_g thus strongly favours the "standard picture". Earlier data did not provide such a critical test, because emulsion data do not have this statistical significance [1] and former counter experiments on nuclei averaged over too broad a distribution in ν, which apparently results in a Z ratio similar to that of hadron-proton collisions.

The advantage of measuring N_g consists, as we said before, in selecting events with a narrower distribution in ν, the number of collisions.

Finally, we want to consider the pseudorapidity distribution as a function of N_g and incoming energy. (The differential multiplicities can obviously give more insight into the mechanism at work than the total multiplicity $\langle N_s \rangle$.) The dominant impression from Fig. 12 is that the change with N_g, i.e. with the number of collisions, is quite different from the predictions of many models. They predict a clear separation of the rapidity distribution into two regions; one above a certain critical rapidity η_c where no change with N_g occurs, and the other below η_c where the change with $\nu = \nu(N_g)$ should be linear. The critical rapidity η_c is predicted to depend only on the energy in some of these (e.g. Gottfried [16]) and only on the size of the nucleus at given impact parameter in other models (e.g. Bertocchi [17]). What we observe is rather a separation into two regions; the upper part showing a depletion and the lower part showing an increase of the number of fast particles; the border η_c between the two regions depends both on the incoming energy and the number of collisions. At first sight it may appear as if the main mechanism reflected in this behaviour is energy conservation and not dynamics. In fact, many models claim to be true only at asymptotically high

energies, and consequently none of these will be challenged by the present data. Some calculations, however, have recently been carried out [18], which will eventually allow a quantitative comparison even at this energy. But work still has to be done on both the theoretical and the experimental side. Concerning the latter a continuation of the experiment at higher energies is planned.

Acknowledgements

We wish to thank Z. Kenesei and J. Zimmer for their continuous technical assistance, and G. Embacher, E. Lorenz, E. Mannheimer, H.G. Ritter, P. Schmidsberger, C. Seemann and W. Zängerling for help at various stages of the experiment.

REFERENCES

[1] A. Gurtu et al., Phys. Lett. 50B (1974) 391.

[2] D.E. Plane, Internal Report CERN/SPS/EA/76-1 (1976).

[3] W. Bozzoli et al., Nucl. Phys. B140 (1978) 271.

[4] I. Otterlund, Proc. 5th Internat. Conf. on High Energy Physics and Nuclear Structure, Uppsala, 1973 (ed. G. Tibell) (North-Holland, Amsterdam, 1973), p. 427.

[5] S.A. Azimov et al., Proc. Topical Meeting on Multiparticle Production on Nuclei at Very High Energies, Trieste, 1976 (eds: G. Bellini, L. Bertocchi and T.G. Rancoita) (Trieste, 1977), IAEA-SMR 21, p. 83.

[6] W. Busza et al., Phys. Rev. Lett. 34 (1975) 839.

[7] A.T. Abrosimov et al., Multiplicity of charged particles in π^- interactions on nuclei at 40 GeV/c, paper submitted to the 19th Internat. Conf. on High-Energy Physics, Tokyo, 1978.

[8] P.K. Malhotra, Nucl. Phys. 46 (1963) 559.

[9] J. Babecki et al., Phys. Lett. B47 (1973) 268.

[10] J. Babecki and G. Nowak, Acta Phys. Pol. B9 (1978) 401.

[11] B. Andersson et al, Phys. Lett. 73B (1978) 343.

[12] B. Andersson and I. Otterlund, Nucl. Phys. B88 (1975) 349.

[13] A. Bialas and W. Czyż, Phys. Lett. 58B (1975) 325.

[14] K. Zalewski, in Proc. Topical Meeting on Multiparticle Production on Nuclei at Very High Energies, Trieste, 1976 (eds: G. Bellini, L. Bertocchi and P.G. Rancoita) (Trieste, 1976), IAEA-SMR 21, p. 145.

[15] Y. Afek et al., in Proc. Topical Meeting on Multiparticle Production on Nuclei at Very High Energies, Trieste, 1976 (eds.: G. Bellini, L. Bertocchi and P.G. Rancoita) (Trieste, 1976), IAEA-SMR 21, p. 591.

[16] K. Gottfried, Phys. Rev. Lett. 32 (1974) 957.

[17] L. Bertocchi, Proc. 6th Internat. Conf. On High Energy Physics and Nuclear Structure, Santa Fe, 1975 (ed. D.E. Nagle et al.) (AIP, New York, 1975), p. 238.

[18] N.N. Nikolaev and V.R. Zoller, preprint CERN TH 2516;
N.N. Nikolaev, A.Ya. Ostapchuk and V.R. Zoller, preprint CERN TH 2541.

Table 1

Relative rates in per cent of projectiles for different incoming momenta measured at a distance of 153 m from the production target

Energy (GeV/c)	π^-	K^-	$\bar{p}$	π^+	K^+	p
20.0	93.4	3.1	3.2	83.7	3.8	12.5
30.0	92.9	4.0	3.1	77.0	4.6	18.4
37.5	93.0	4.2	2.8	72.2	5.8	22.0

Table 2

Typical counting rates for a target with 1% absorption length thickness

B • S (full size beam)	280,000 per pulse $\sim 10^6$ per sec
B • S • D • $\bar{A}_H$ • $\bar{C}_1$ = "Beam"	10^4 per pulse
"Beam" • "Or"	265 per pulse
Computer dead-time	30 %
Accepted triggers	185 per pulse
A_B rejected	55 per pulse
Written on tape	130 per pulse
Good events	80 per pulse
Interactions	0.012 per "Beam"

Figure captions

Fig. 1 : The detector: (1) photomultiplier, (2) lucite, (3) CsI(Tl) crystal. The layout of the beam counters is shown on top.

Fig. 2 : Angular distribution of fast and slow particles. Arrows on the horizontal axis indicate counter positions. Different curves for slow particles belong to different energy losses in the CsI, measured in units of the energy loss ΔE of a minimum ionizing particle.

Fig. 3 : a) Frequency of events $f(N_g, A)$ versus number of observed slow particles for different targets and incoming π^- of 37.5 GeV/c.

b) Frequency of events $f(N_s, A)$ versus number of observed fast particles.

Fig. 4 : a) Energy independence of $f(N_g, A)$. For the definition of $R(N_g)$ see Eq. (4).

b) Energy dependence of $f(N_s, A)$. For the definition of $R(N_s)$ see Eq. (6).

$R(N_g)$ and $R(N_s)$ are normalized to unity at low multiplicity.

Fig. 5 : Mean values $\langle N_s \rangle$ and $\langle N_g \rangle$ versus $\bar{\nu}$ as a function of the average number of collisions $\bar{\nu}$ for different nuclei.

Fig. 6 : a) Average pseudorapidity distribution of fast particles for different targets at 37.5 GeV/c (π^-, K^-).

b) Energy dependence of the pseudorapidity distributions for different targets. The ratio R is defined in Eq. (8).

Fig. 7 : Dependence of the pseudorapidity distributions on $\bar{\nu}$:

a) for π^- (20 GeV/c);

b) for π^- (37.5 GeV/c).

Fig. 8 : Increase of secondaries in subsequent collisions as a function of the pseudorapidity. $S(\eta)$ is defined in Eq. (7).

Fig. 9 : Frequency distribution of events $f(N_s, N_g)$ versus observed N_s. Curves are for different observed N_g. π^- + Pb at 37.5 GeV/c.

Fig. 10 : Normalized dispersion of fast particles a) as a function of $\langle N_s \rangle$ and b) as a function of N_g. For the definition of $Z = \langle D \rangle / \langle N_s \rangle$ see Eq. (9).

Fig. 11 : Dependence of the mean number $\langle N_s \rangle$ of fast particles on the number N_g of slow particles.

Fig. 12 : The pseudorapidity distribution as a function of the number of observed slow particles N_g for π^- + Pb a) at 20 GeV/c, b) at 37.5 GeV/c.

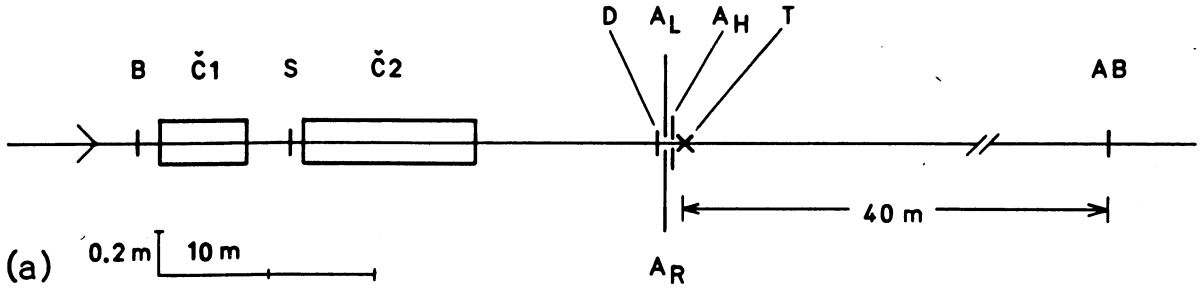
D
A_L
A_H
T
B
Č1
S
Č2
AB
40 m
(a)
0.2 m
10 m
A_R

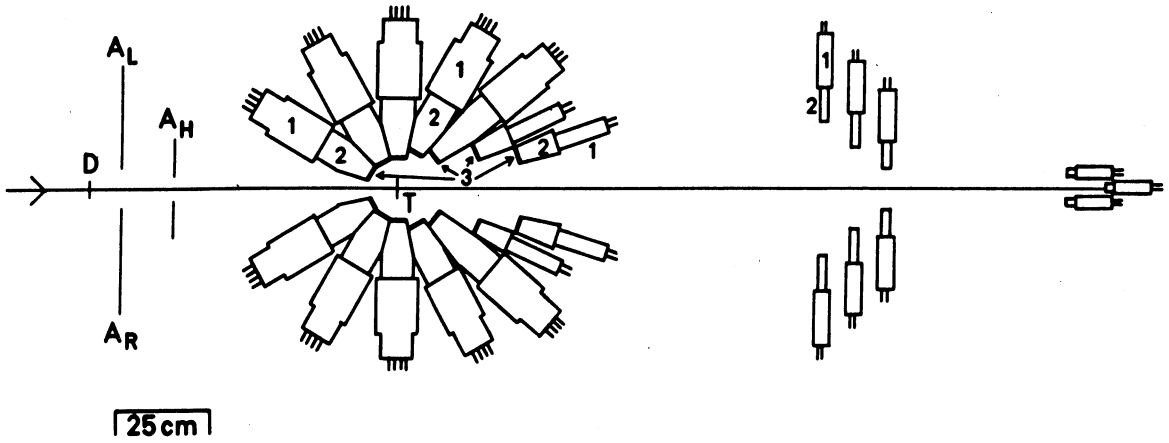
A_L
A_H
D
T
A_R
1
2
3
25cm
(b)
73 Cs I + Lucite counters
48 Lucite
7

Fig. 1

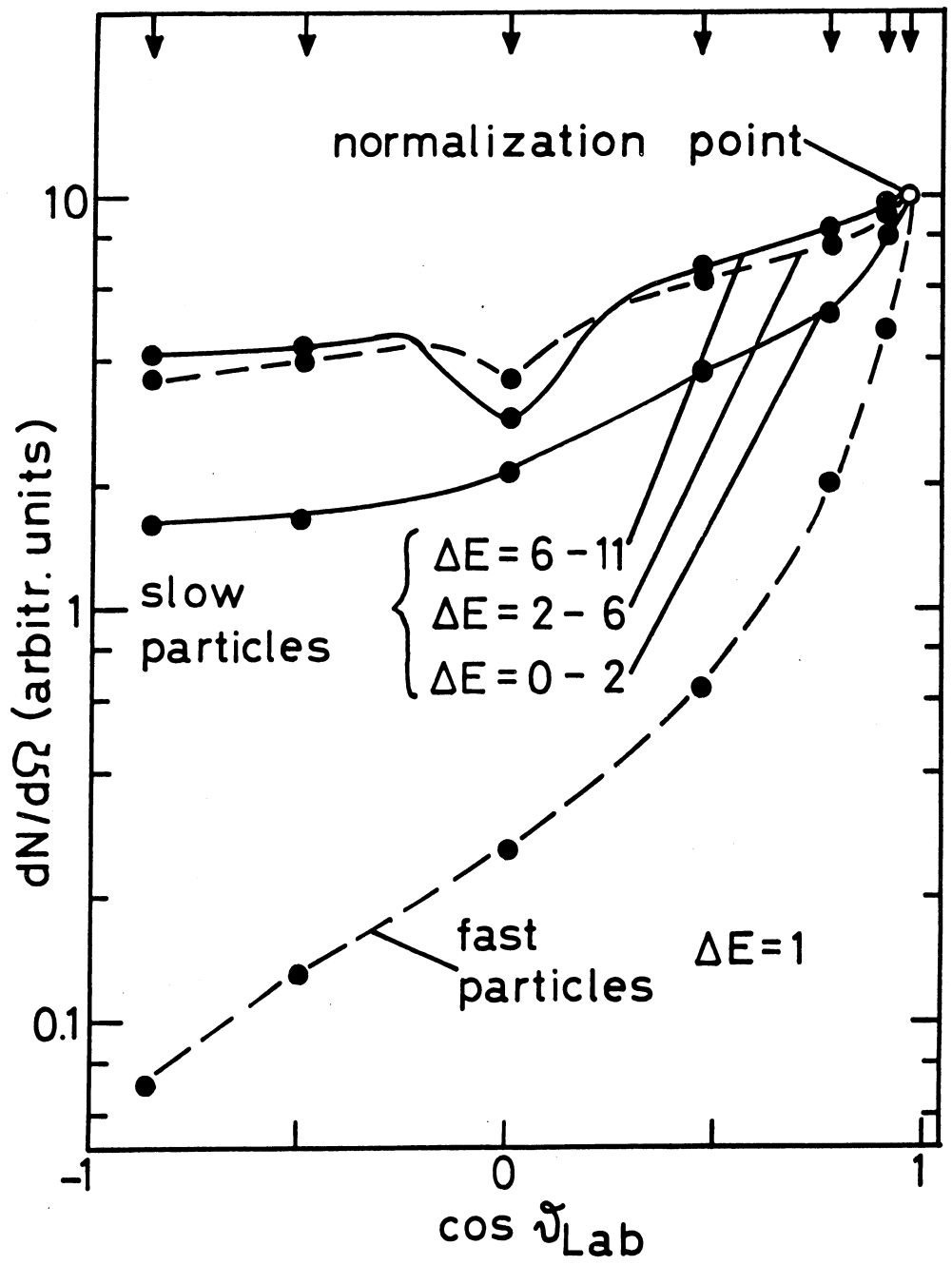
normalization point
10
1
0.1
dN/dΩ (arbitr. units)
slow
particles
ΔE = 6 - 11
ΔE = 2 - 6
ΔE = 0 - 2
fast
particles
ΔE=1
-1
0
1
cos ϑLab

Fig. 2

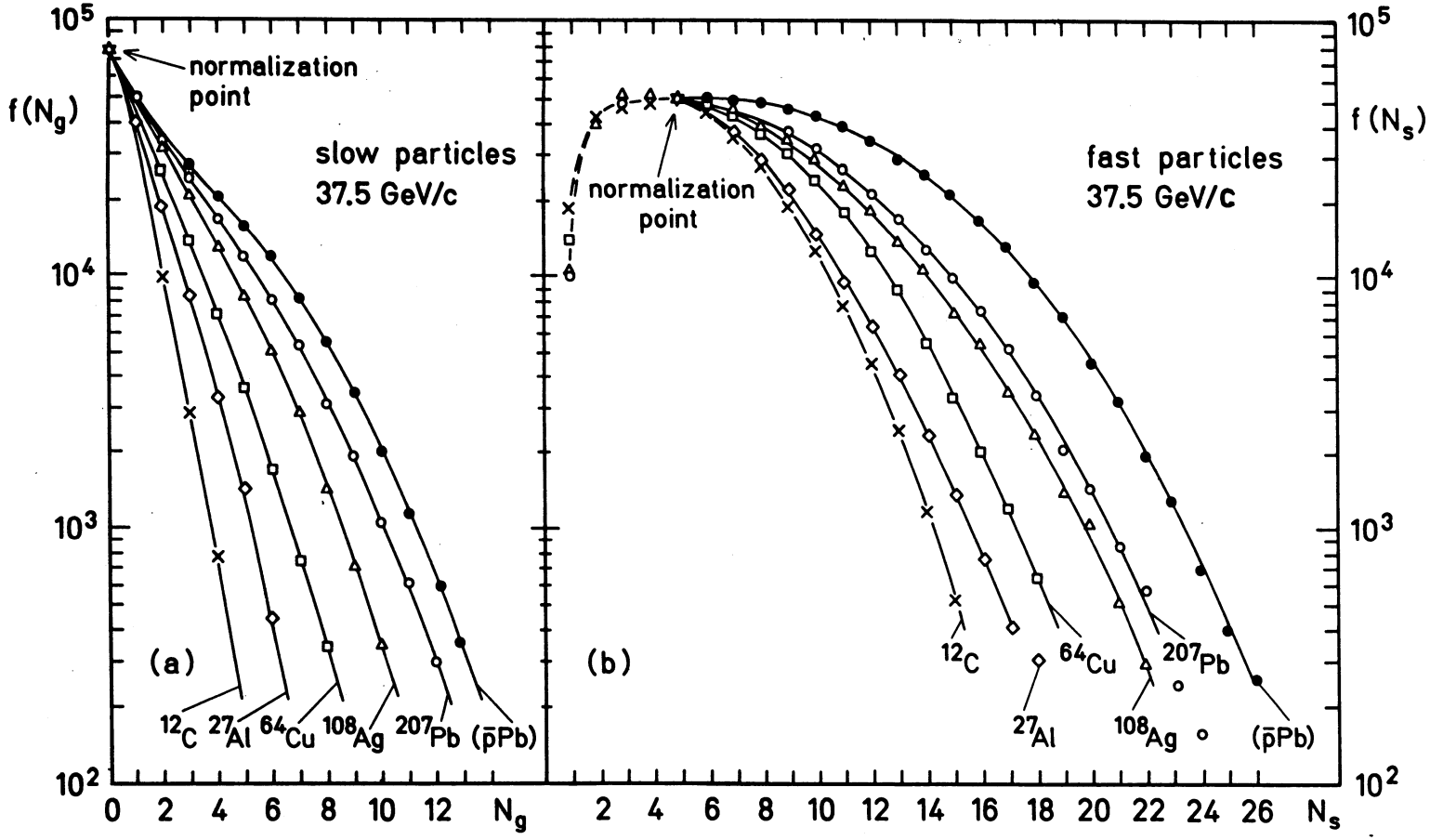
normalization point
slow particles
37.5 GeV/c
f(N_g)
(a)
12C 27Al 64Cu 108Ag 207Pb (p̄Pb)
N_g
normalization point
fast particles
37.5 GeV/c
f(N_s)
(b)
12C
27Al
64Cu
108Ag
207Pb
(p̄Pb)
N_s

Fig. 3

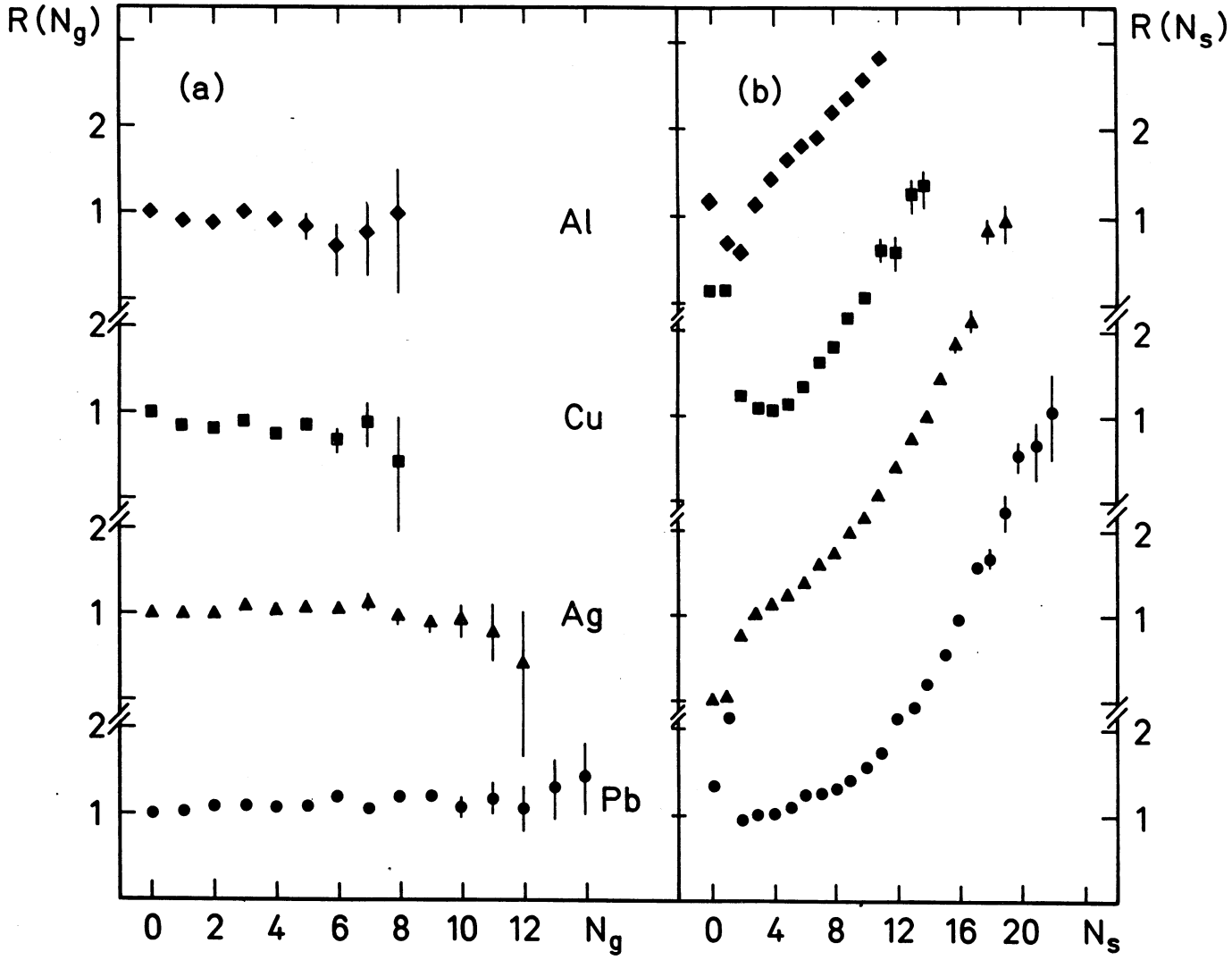

Fig. 4

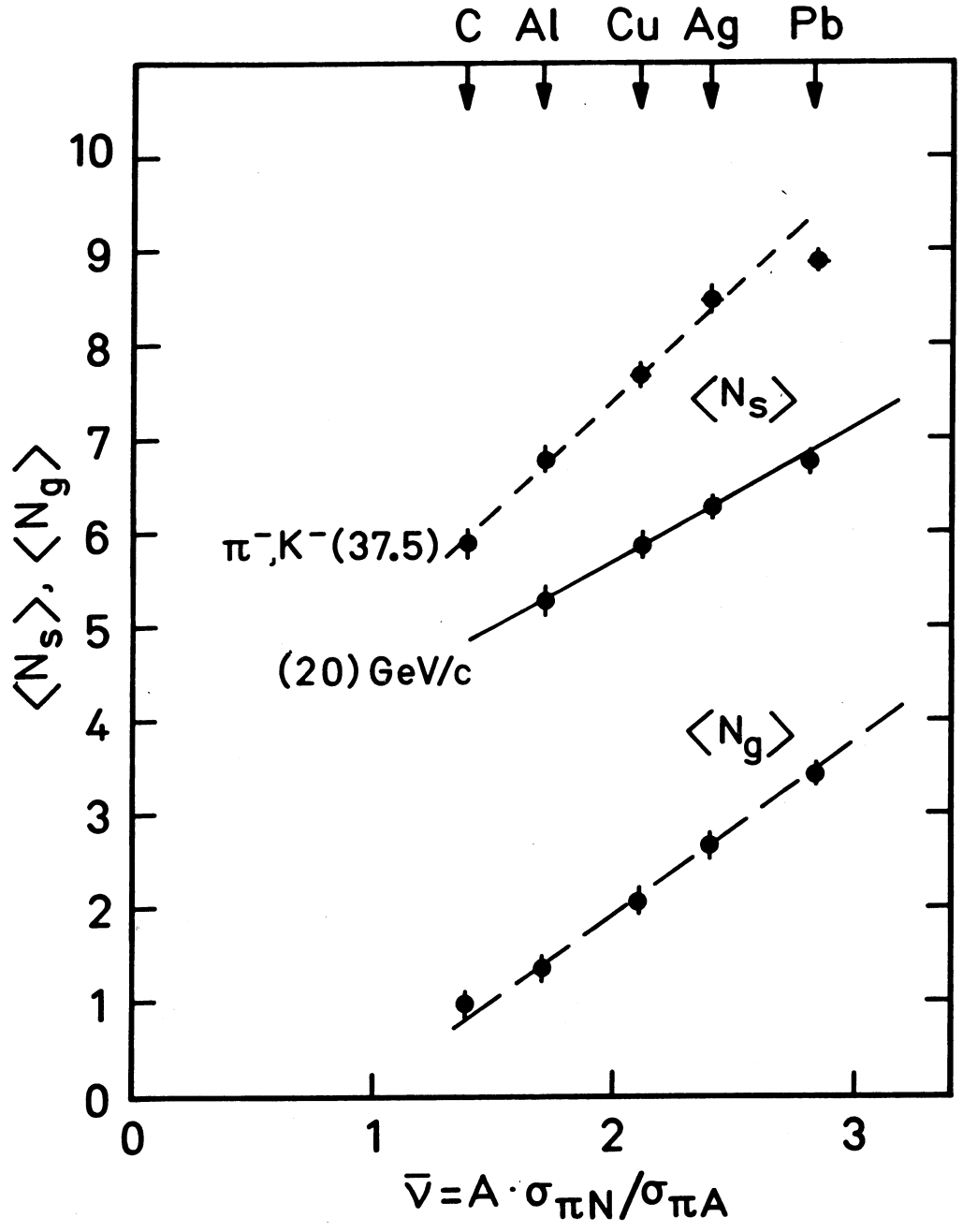
C Al Cu Ag Pb
10
9
8
7
6
5
4
3
2
1
0
0
1
2
3
⟨Ns⟩, ⟨Ng⟩
⟨Ns⟩
π⁻,K⁻(37.5)
(20) GeV/c
⟨Ng⟩
ν̄ = A · σπN/σπA

Fig. 5

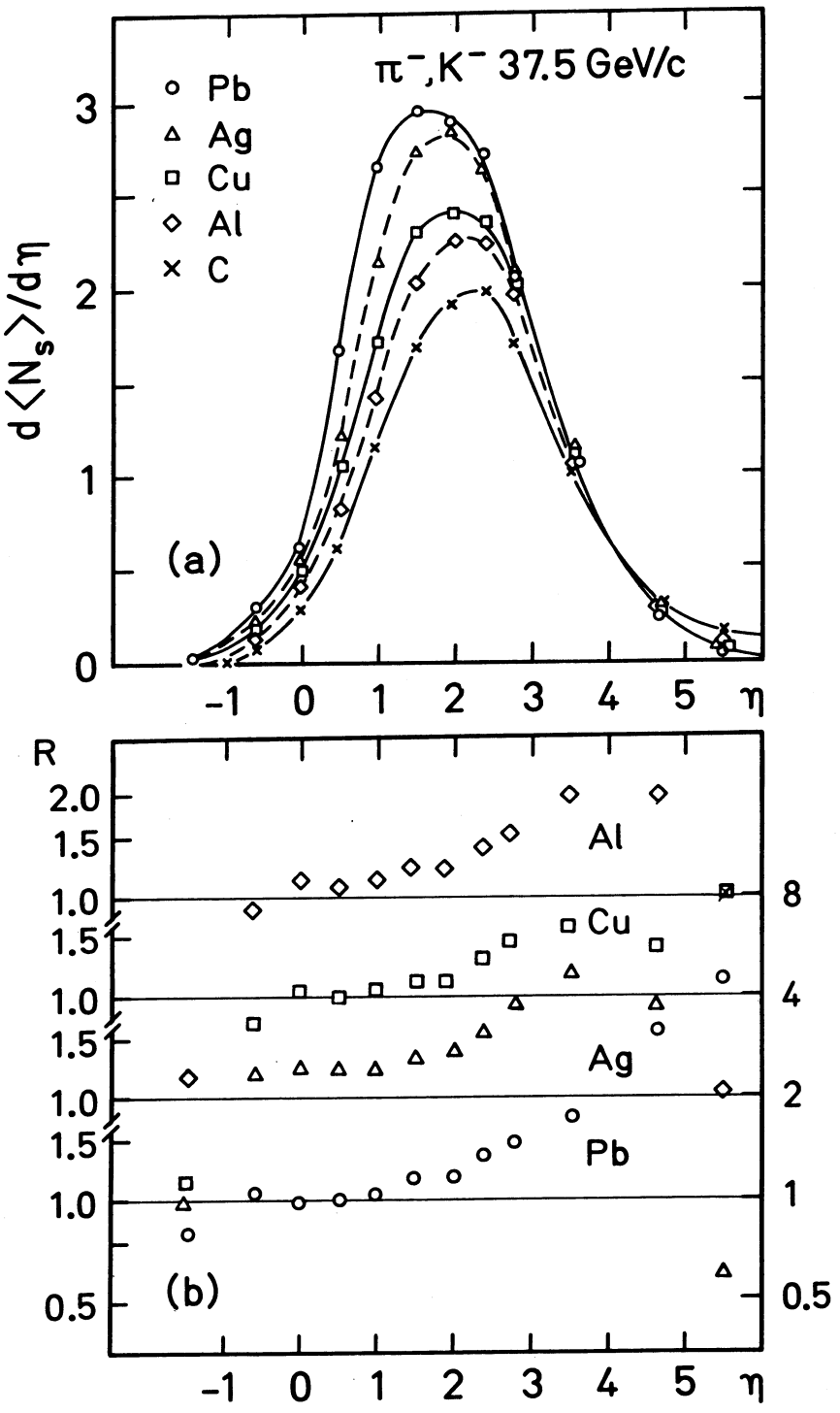

Fig. 6

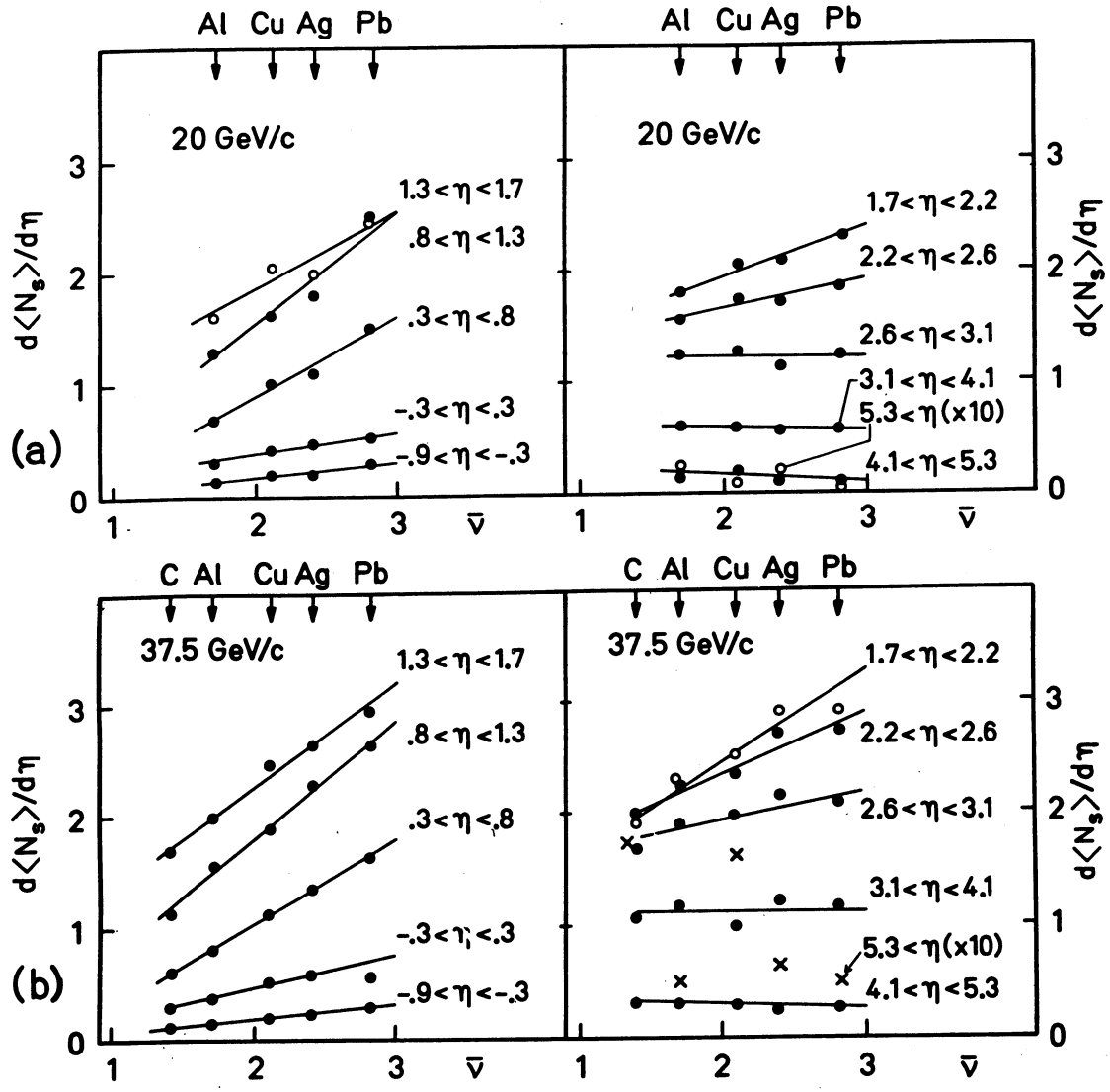
Al Cu Ag Pb
20 GeV/c
1.3<η<1.7
.8<η<1.3
.3<η<.8
-.3<η<.3
-.9<η<-.3
(a)
1.7<η<2.2
2.2<η<2.6
2.6<η<3.1
3.1<η<4.1
5.3<η(x10)
4.1<η<5.3
C Al Cu Ag Pb
37.5 GeV/c
(b)
d⟨Ns⟩/dη
ν̄

Fig. 7

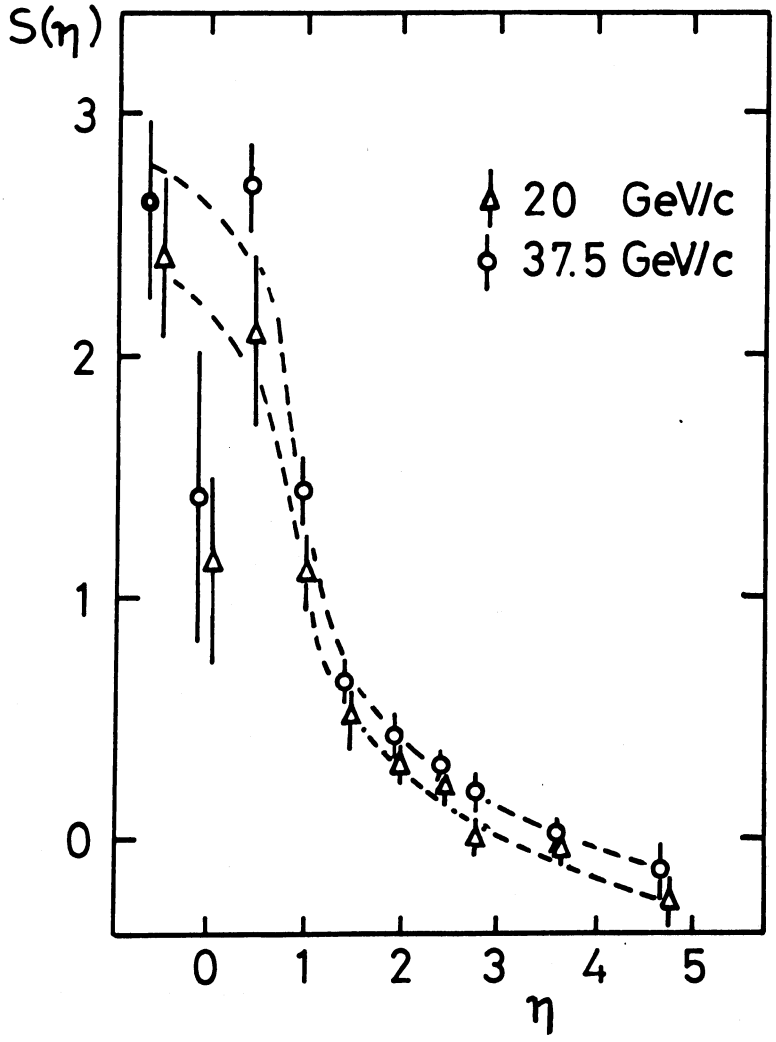

Fig. 8

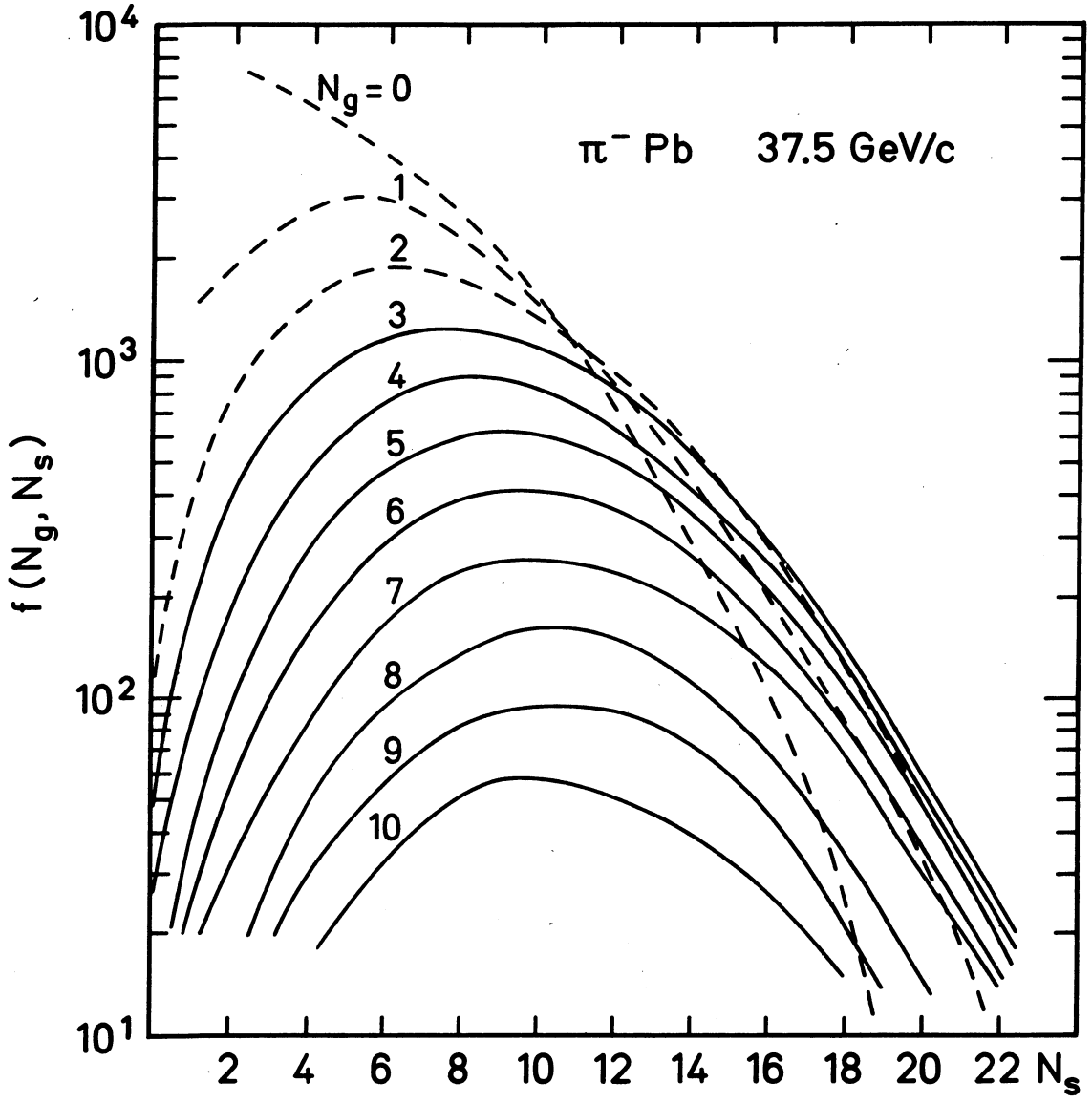
10^4
10^3
10^2
10^1
$f(N_g, N_s)$
$N_g = 0$
1
2
3
4
5
6
7
8
9
10
π^- Pb 37.5 GeV/c
2 4 6 8 10 12 14 16 18 20 22 N_s

Fig. 9

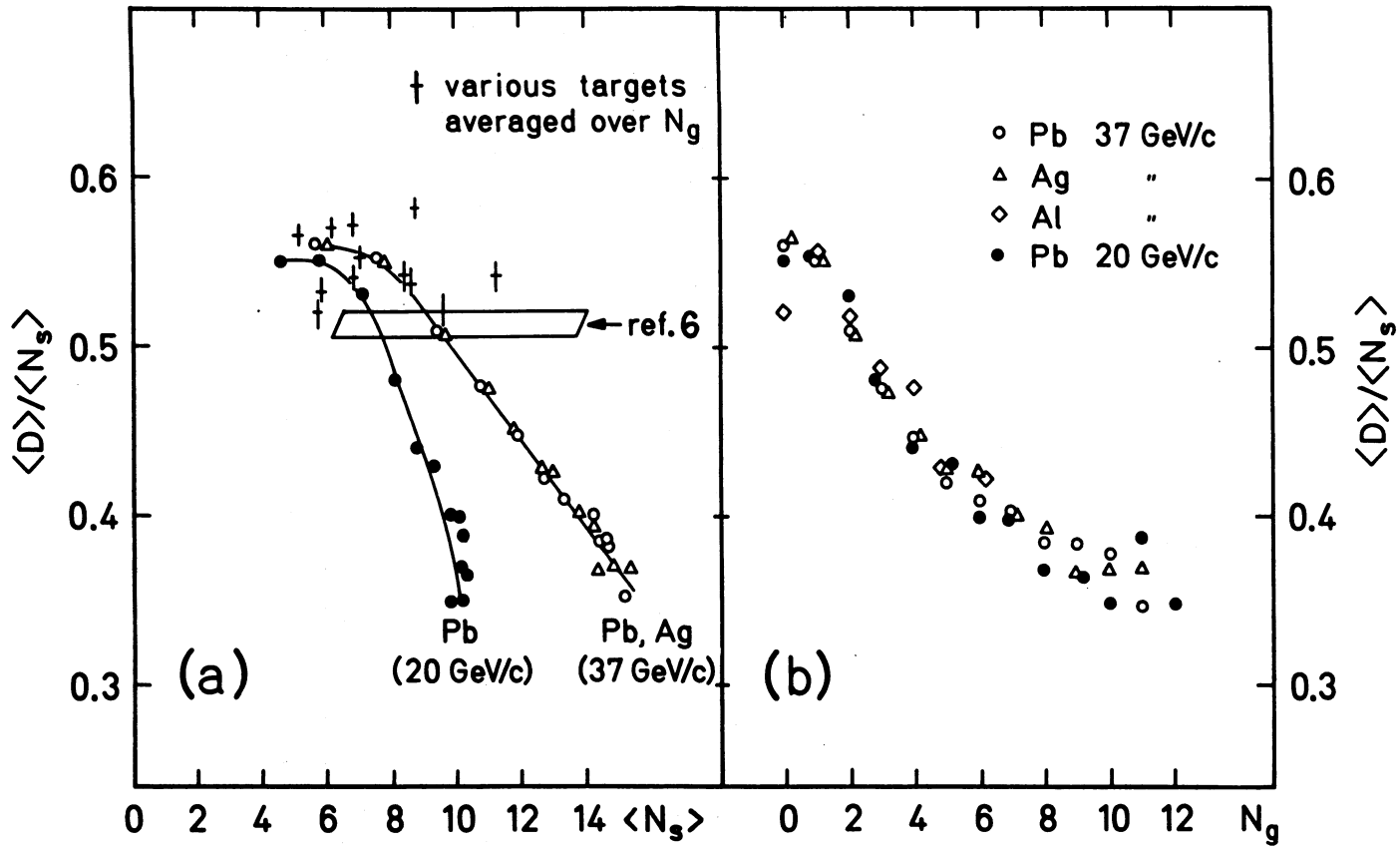
† various targets
averaged over N_g
ref. 6
Pb
(20 GeV/c)
Pb, Ag
(37 GeV/c)
(a)
(b)
Pb 37 GeV/c
Ag "
Al "
Pb 20 GeV/c
$\langle D \rangle / \langle N_s \rangle$
$\langle N_s \rangle$
N_g
0.3
0.4
0.5
0.6
0 2 4 6 8 10 12 14
0 2 4 6 8 10 12

Fig. 10

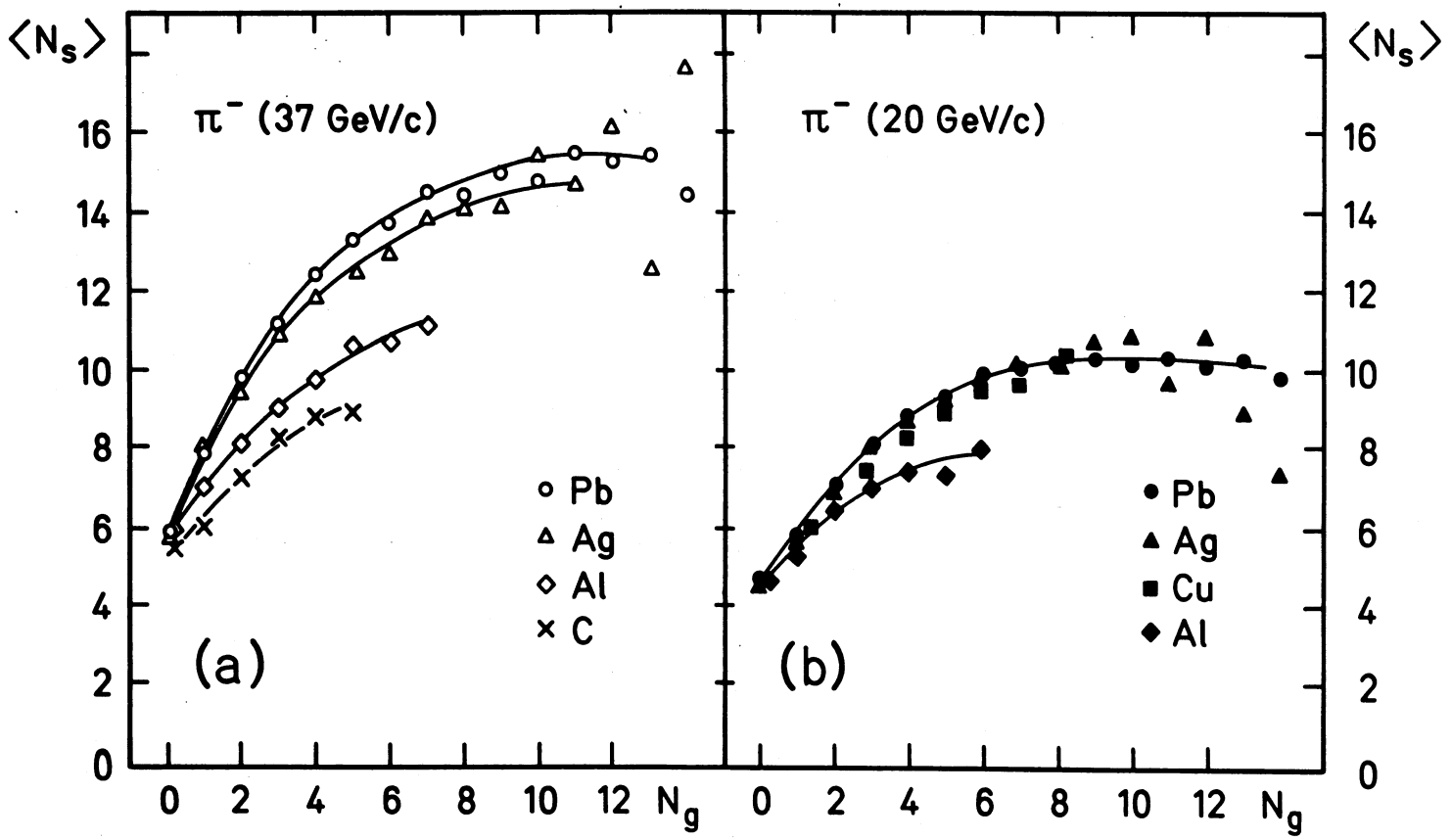

Fig. 11

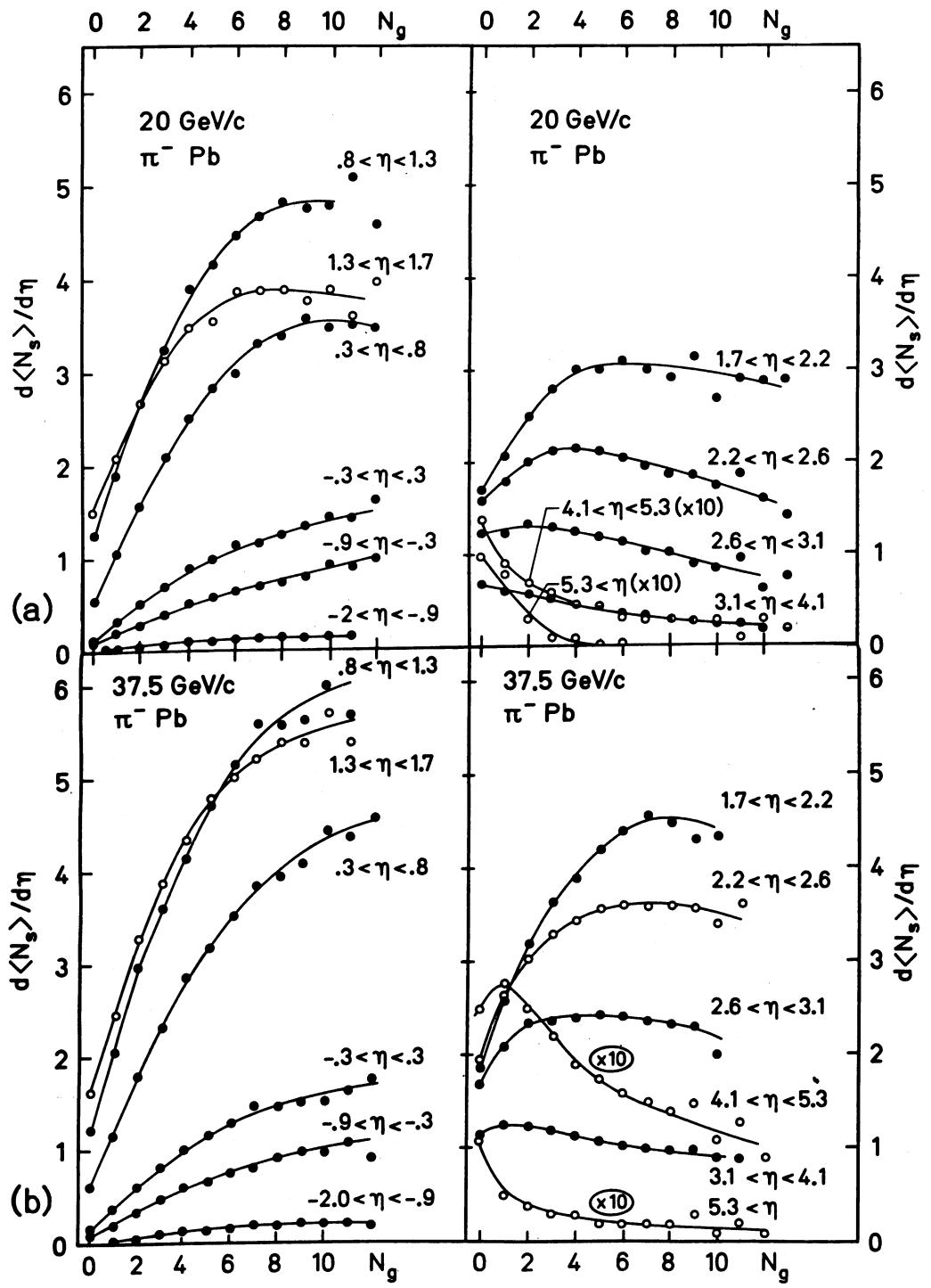
0 2 4 6 8 10 N_g
20 GeV/c
π^- Pb
.8<η<1.3
1.3<η<1.7
.3<η<.8
-.3<η<.3
-.9<η<-.3
-2<η<-.9
(a)
1.7<η<2.2
2.2<η<2.6
4.1<η<5.3 (x10)
2.6<η<3.1
5.3<η (x10)
3.1<η<4.1
37.5 GeV/c
π^- Pb
.8<η<1.3
1.3<η<1.7
.3<η<.8
-.3<η<.3
-.9<η<-.3
-2.0<η<-.9
(b)
1.7<η<2.2
2.2<η<2.6
2.6<η<3.1
(x10)
4.1<η<5.3
3.1<η<4.1
(x10)
5.3<η
$d\langle N_s\rangle/d\eta$

Fig. 12